Prepared for submission to JINST

Monte Carlo simulation of HERD side-on transition radiation detector prototype

Cong Dai,[a] **Hongbang Liu,**[a,1] **Ming Xu,**[b] **Huanbo Feng,**[a] **Fei Xie,**[a] **Xiwen Liu,**[a] **Yongbo Huang,**[a] **Xiang Lu,**[a] **Yongwei Dong,**[b] **Enwei Liang**[a]

[a] *Guangxi Key Laboratory for Relativistic Astrophysics, School of Physical Science and Technology, Guangxi University, 100 Daxue East Road, Nanning, China*

[b] *Key Laboratory of Particle Astrophysics, Institute of High Energy Physics, Chinese Academy of Sciences, 19B Yuqyan Road, Beijing, China*

E-mail: liuhb@gxu.edu.cn

Abstract: The High Energy cosmic-Radiation Detection facility (HERD) is a calorimetry-based cosmic-ray detection mission on board China space station. A side-on transition radiation detector (TRD) focuses on the TeV energy range calibration of the HERD calorimeter with an error of less than 10% by measuring the Lorentz factor γ of high-energy cosmic-ray protons. A side-on TRD prototype was developed for the performance study and tested by Deutsches Elektronen-Synchrotron electron beams. In this paper, the Monte Carlo simulation based on GEANT4 was compared with the experiment results. All simulations were in good agreement with the test beam results.

Keywords: Transition Radiation Detector, Thick-Gas Electron Multiplier, GEANT4 Simulation

[1] Corresponding author.

Contents

1 Introduction

The High Energy cosmic-Radiation Detection facility (HERD) [1–4] is a space astronomy payload that will be installed on board China space station for 10 years of operation. HERD comprises five types of detectors: the calorimeter (CALO), fiber tracker, plastic scintillator, silicon charge detector and transition radiation detector (TRD). The TRD is a sub-detector used for TeV energy calibration in orbit that can improve cosmic-ray energy measurement precision.

Transition radiation (TR), which was predicted by Frank and Ginzburg [5], is one electromagnetic wave emitted by a relativistic charged particle when the particle crosses the interface between two media with different dielectric constants. TR has several characteristics: (1) the energy of emergent TR-photons from the radiator usually is in the soft X-ray energy range because of the low energy photon absorbed by the radiator; (2) the TR-photon yield of a single-layer interface is of the order of 1/137; (3) the TR emission angle is small, and the maximum probability is $\theta = 1/\gamma$; (4) the response curve between the TR intensity (which can be expressed as the number of TR-photons or the total TR energy deposition) and the Lorentz factor γ of the incident-charged particle can be divided into three parts: threshold region, linear region and saturation region. It has significant TR from $\gamma_{\rm thr} \simeq 2.5\hbar\omega_{\rm p1}l_1$ [6], and the TR intensity reaches saturation at $\gamma_{\rm sta} \simeq 3.0\hbar\omega_{\rm p1}\sqrt{l_1 l_2}$, where $\hbar$ is the reduced planck constant, $\omega_{\rm p1}$ is the plasma frequency of radiator foil, l_1 and l_2 are the thickness of radiator foil and gap. The TR intensity is proportional to γ in the linear region. The linear range is between 10^3 and 10^4, for the typical radiator composed of plastic and gas gap. Traditional TRD has two kinds: straw tube TRD and multi-wire proportional chamber (MWPC) TRD [7, 8]. They are major used for particle identification and γ measurement in accelerator experiments and astronomical experiments.

The side-on TRD was designed for the HERD space mission focuses on the TeV energy range calibration of the HERD CALO, which is a time projection chamber (TPC) based on the thick-gas electron multiplier (THGEM). The transition radiator was installed on the lateral face of the TPC, and the trajectory of a particle was parallel to the anode plane and perpendicular to the electric field in the drift region, as shown in figure 1(a). The method of achieving energy calibration is by taking advantage of the effective cosmic-ray protons in the TeV energy region triggered by TRD and CALO

simultaneously, and the expected calibration accuracy is within 10%. The calibration accuracy is related to the slope of the detector response curve and the uncertainty of the TR signal [6].

A side-on TRD prototype was developed and its performance was studied by using electron beams. We tested the properties of different working gases and the performance of THGEM with various parameters by using the ^{55}Fe source [9]. The regular radiator parameters were optimized using a fast calculating program [10] and were tested using electron beams [11]. To optimize the detector and study its in-orbit calibration performance, an Monte Carlo (MC) model is required. Although there have been studies on the simulation of straw tube TRD and MWPC TRD [12–15], few simulations of THGEM TRD have been conducted. In this work, we constructed an MC model based on the electron characteristics of transverse diffusion in the drift region and multiplication in the THGEM hole, and compared the simulation results with the test beam results. We used the verified MC model to optimize the detector design, and compared the optimized results with the prototype. This paper is organized as follows: section 2 describes the experimental setup, section 3 presents the simulation construction and comparison of GEANT4 and test beam results, section 4 represents the detector optimization, and finally, the conclusion is presented in section 5.

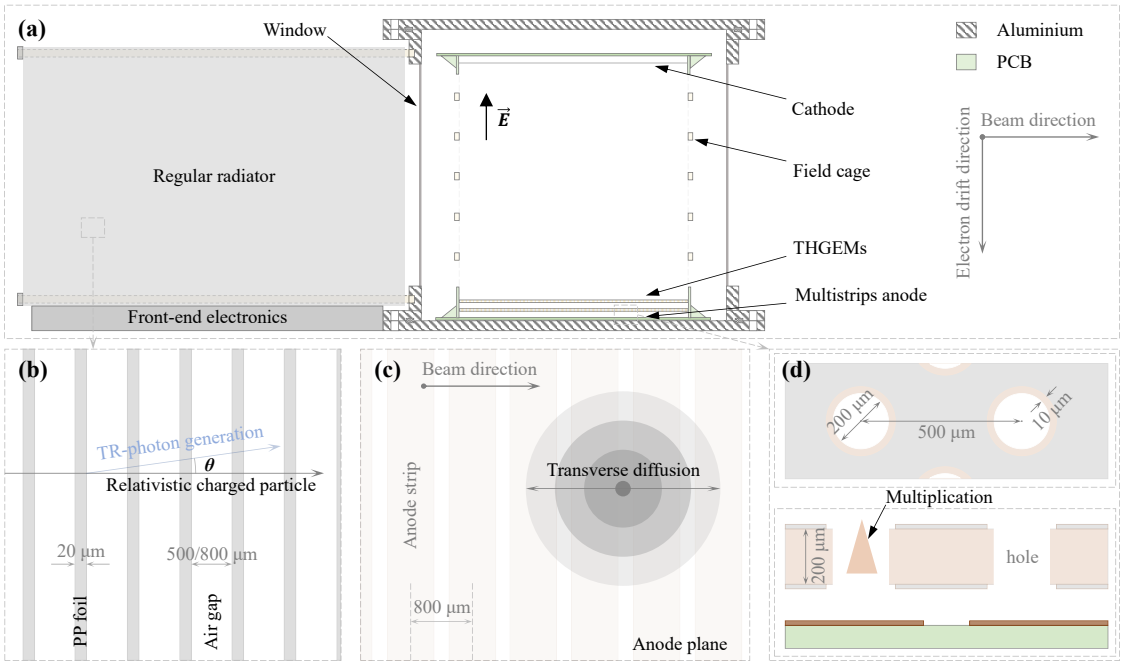

Figure 1: (a) Profile of the side-on TRD prototype; (b) structure of the regular radiator; (c) transverse diffusion projected onto the anode plane; (d) THGEM parameters (top) and the multiplication of electron in the THGEM hole (bottom).

2 Experimental setup

The side-on TRD consisted of a regular radiator, a gas detector based on double-layer THGEMs, and multi-readout electronics. The detector profile was shown in figure 1(a), where the structures from left to right were the regular radiator, incident window, and gas chamber. The front-end electronics were installed under the regular radiator. Two regular radiators were composed of 20-μm thick polypropylene (PP) foils arranged in 500/800-μm thick air gaps with 300/225 layers, as shown in figure 1(b). The gas chamber included the cathode, field cage, two THGEMs (the geometry parameters of THGEM were labeled in figure 1(d)), and anode with 64 readout strips (650 μm wide and 150 μm in-between). The electronics [16] used the multi-channel readout system, comprising

the front-end cards (FECs) and a data collection module. The FEC utilized the AGET chip, with 64 channels. The switched capacitor array structure of each channel enabled the waveform readout, and each channel had 512-sample analogue memory. The maximum charge the amplifier could transmit and the sampling frequency were selected as 120 fC and 25 MHz, respectively.

The gas chamber was filled with Ar/CO_2 at a mixing ratio of 93:7 at atmospheric pressure, and the chamber window had an area of 5×5 cm^2. In the drift region, the electric field was 450 V/cm, provided by the field cage. The voltage difference between the upper and lower surfaces of each THGEM layer was 680 V. The detector was tested on electron beams from Deutsches Elektronen-Synchrotron (DESY) [17] (the beam size was 1×1 cm^2 and the energy divergence was 5%) ranging from 1.0 to 5.6 GeV/c. The detection principle describes the relativistic charged particle that passed through the regular radiator and produced the TR-photon (figure 1(b)). These two types of particles, the incident-charged particle, and the TR-photon, arrived in the sensitive volume of the gas chamber at approximately the same time. The TR-photon interacted with the working gas through the photoelectric effect, which was dominant at soft X-rays. The photo-electron and the incident-charged particle deposited energy through ionization in the drift region. The ionized electrons of the two aforementioned signals drifted toward the THGEM, multiplied in the THGEM holes, and were collected by the anode strips (figure 1(d)).

3 Simulation and comparison with the test beam results

3.1 Simulation construction

An MC simulator based on GEANT4.10.03 was constructed and used to reproduce the test beam results. All structures and material descriptions in the MC simulation were consistent with the physical detector. The electrons were generated according to the beam configuration. The simulation addressed several major physical processes. The existing TR model G4TransparentRegXTRadiator [18] in GEANT4 described the TR physics process of relativistic charged particles in the regular radiator. The Photo Absorption Ionization model (G4PAIModel) [19] reproduced the energy loss of relativistic charged particles in thin gas, and the G4VAtomDeexcitation described the Auger electron emission and characteristic X-ray process of atomic deexcitation.

3.2 Transverse diffusion coefficient and digitization model

The ionization electrons transverse diffusely during the drifting process in the drift region. The two-dimensional transverse diffusion is projected onto the anode plane, where only the one-dimensional, along the beam direction, diffusion perpendicular to the anode strip needs to be considered, as shown in figure 1(c). A Gaussian distribution with a standard deviation of σ_x along the beam direction can describe the ionization electron dispersion. For an arbitrary drift distance of L, σ_x is given by the following equation:

$$\sigma_x = D_T \cdot \sqrt{L}$$

where D_T is the transverse diffusion coefficient and is expressed in $\mu m/\sqrt{cm}$. This parameter was 330 $\mu m/\sqrt{cm}$ for the mixture gas $Ar:CO_2(93:7)$ according to Garfield++ [20].

The simulation's digitized input is obtained from Geant4's recorded hit position and energy, and its output is the ADC value of the detector's multi-readout channel. As described above, ionized electrons are produced and then drift toward the anode in the drift region. We calculate the drift distance L and diffusion width σ_x by using the hit position. Each hit allocates deposition energy to a different readout channel according to the Gaussian function with a standard deviation σ_x. The electrons are multiplied in the THGEM hole with a gain coefficient of 182 ADC/keV, and the energy

broadening caused by THGEM is described by a Gaussian function with an FWHM of 31% at 5.9 keV. The anode collects all the multiplied electrons, and there is an offset for electronics response, with a value of -9 ADC. Laboratory tests can get all of the above parameters by using a ^{55}Fe source. More detailed discussions on the test can be found in ref. [9].

3.3 Comparisons of the simulation and the test beam results

The energy spectra of the simulation and the test beam results were compared using the following method. For each event, one of the anode strips with the highest energy deposition contributed by the TR-photon or the delta electron was selected. The readout strips on both sides of the field cage were excluded due to the uneven electric field causing margin effects. From the middle 30 readout strips, the strip with the largest energy deposition was selected as the center, and two readout strips were added to each side. The sum of the signals on the five readout strips was considered the deposited energy for that event. Summing all the signals on the anode strips would drown out the TR signal. Although the energy deposited by the TR photo-electron was distributed over several consecutive strips due to transverse diffusion, the energy deposited using the above method contains most of the energy from a single TR photo-electron.

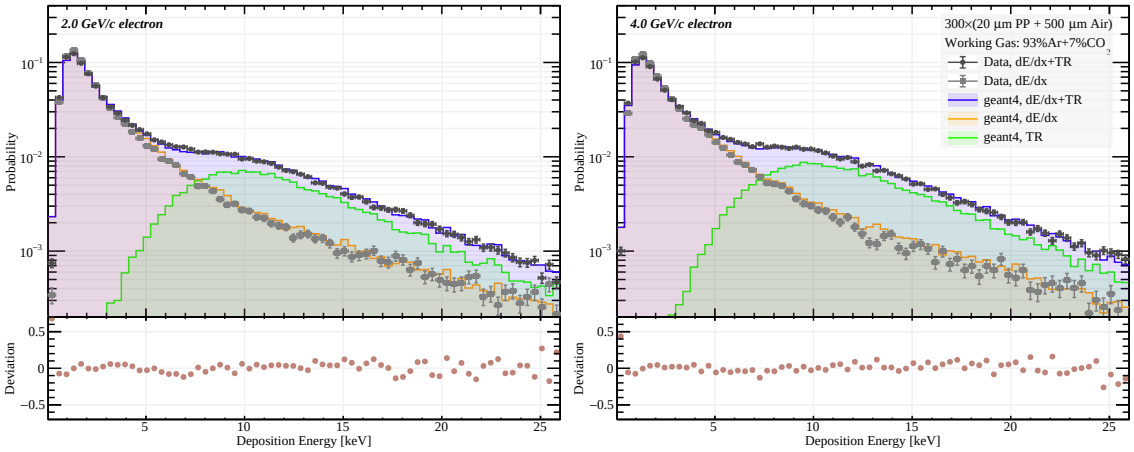

Figure 2: TR and ionization spectra of the simulation and test beam results. The momenta of the beam electrons from left to right are 2.0 and 4.0 GeV/c, respectively. The black circle represents the measured TR + ionization spectrum; the gray square is the measured ionization spectrum; the blue line represents the simulated TR + ionization spectrum; the orange line represents the simulated ionization spectrum; the green line represents the simulated TR contribution. The bottom two panels show the corresponding deviation between data and MC. Radiator parameters are 300×(20 μm PP + 500 μm Air).

figure 2 presents the ionization spectra of 2 and 4 GeV/c electrons for both simulation and test beam results. The simulations were consistent with the test beam results for different electron momenta. Two types of regular radiators were simulated and tested. The first radiator parameter consisted of 300 layers of foil with a gap of 500 μm. TR spectra of electron momenta from 2.0 to 5.6 GeV/c were obtained and presented in figures 2 and 3. The second radiator parameter consisted of 225 layers of foil with a gap of 800 μm, and figure 4 shows the corresponding TR spectra. All simulation and test beam results were consistent.

3.4 The TR-photon yield

The TR-photon yield, which refers to the average number of TR-photons emitted from the radiator after taking into account the self-absorption of the radiator, can be determined by deconvoluting the

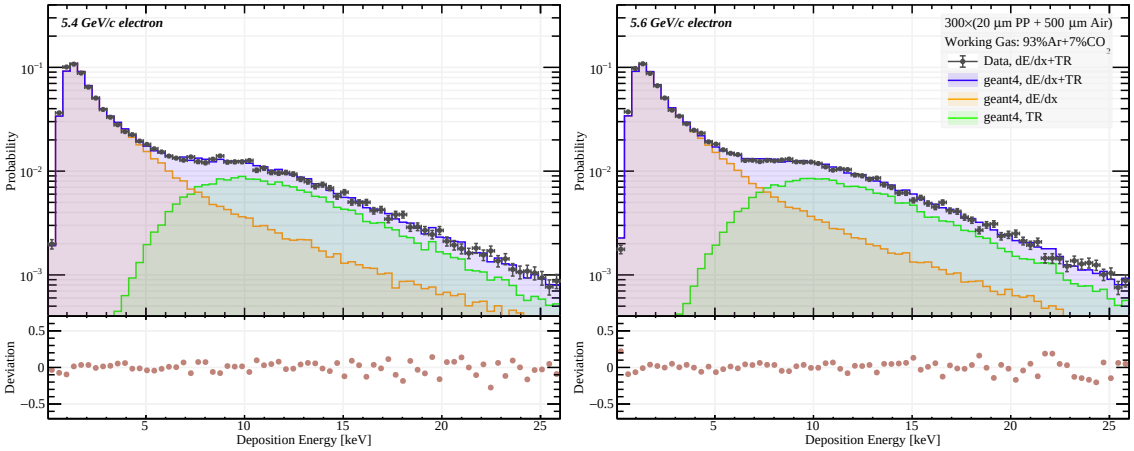

Figure 3: TR and ionization spectra of the simulation and test beam results. The momenta of the beam electrons from left to right are 5.4 and 5.6 GeV/c, respectively. The four histograms represent the same meaning as figure 2. Radiator parameters are 300×(20 μm PP + 500 μm Air).

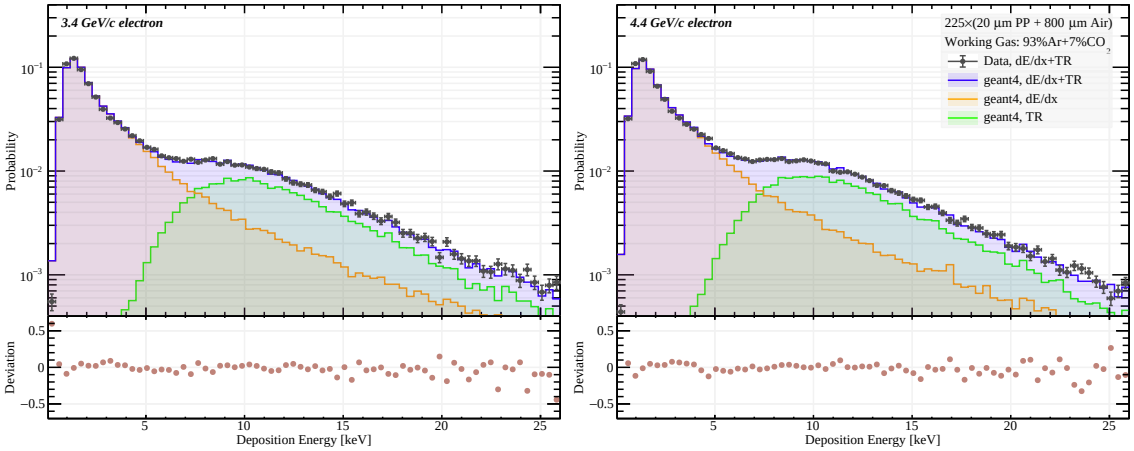

Figure 4: TR and ionization spectra of the simulation and test beam results. The momenta of the beam electrons from left to right are 3.4 and 4.4 GeV/c, respectively. The four histograms represent the same meaning as figure 2. Radiator parameters are 225×(20 μm PP + 800 μm Air).

measured TR signal using the detector detection efficiency. Table 1 lists the simulated and measured TR-photon yields for the two regular radiators, and the simulation and measurement results are in agreement. The average TR-photon yield for the two radiators in the saturated region was 4.8 and 4.6, respectively.

4 Detector optimization

We optimize the detector design by using the verified MC model. Specifically, the calibration accuracy of the TRD, denoted by σ_γ, is determined by the system uncertainty $\sigma_{\mathfrak{R},\mathrm{sys}}$ and the statistical uncertainty $\sigma_{\mathfrak{R},\mathrm{sta}}$ of the measured TR signal, as well as the slope of the TR response curve $\mathfrak{R}'(\gamma)$ [6], which can be written as:

$$\sigma_\gamma = \sqrt{\sigma^2_{\mathfrak{R},\mathrm{sys}} + \sigma^2_{\mathfrak{R},\mathrm{sta}}}/\mathfrak{R}'(\gamma)$$

We can reduce the system uncertainty by improving the gain uniformity and stability of the detector. To reduce statistical uncertainty, we can optimize the geometric parameters of the detector to improve the statistics of effective proton events. One way to achieve this is by increasing the number

Table 1: Average TR-photon number emergent from the radiator with different electron momenta P_{e^-}.

P_{e^-} (GeV/c)	300×(20 μm PP + 500 μm Air)		225×(20 μm PP + 800 μm Air)	
	Simulation	Measured*	Simulation	Measured*
1.0	1.68	$1.68^{+0.01}_{-0.01}$	1.45	$1.48^{+0.01}_{-0.01}$
1.4	3.01	$2.92^{+0.03}_{-0.03}$	2.22	$2.28^{+0.03}_{-0.02}$
2.0	4.00	$3.99^{+0.04}_{-0.03}$	3.40	$3.53^{+0.04}_{-0.02}$
2.4	4.30	$4.28^{+0.05}_{-0.04}$	3.81	$3.82^{+0.04}_{-0.03}$
3.0	4.57	$4.54^{+0.07}_{-0.04}$	4.18	$4.33^{+0.04}_{-0.03}$
3.4	4.67	$4.68^{+0.06}_{-0.05}$	4.32	$4.40^{+0.04}_{-0.04}$
4.0	4.77	$4.75^{+0.06}_{-0.05}$	4.46	$4.62^{+0.04}_{-0.04}$
4.4	4.82	$4.88^{+0.06}_{-0.04}$	4.52	$4.57^{+0.05}_{-0.03}$
5.2	4.88	$4.84^{+0.08}_{-0.05}$	4.62	$4.69^{+0.05}_{-0.04}$
5.4	4.89	$4.84^{+0.07}_{-0.05}$	4.63	$4.63^{+0.05}_{-0.04}$
5.6	4.90	$4.85^{+0.06}_{-0.04}$	4.64	$4.68^{+0.04}_{-0.03}$

* The maximum system uncertainty σ_{sys} was estimated to be 1.42% according to the simulation. The total measurement deviation was expressed in $\sigma = \sqrt{\sigma_{\text{sys}}^2 + \sigma_{\text{sta}}^2}$, and the maximum is 1.56%, where σ_{sta} is the statistic uncertainty.

of detectable TR-photons per event. The slope of the response curve of TRD is positively correlated with the number of detectable TR-photons, which plays a crucial role in improving the calibration accuracy.

To improve the number of detectable TR-photons, we optimized the detector design from the following aspects:

- The radiator is installed inside the chamber, which avoids the problem of pressure difference between the inside and outside of the detector when using thin windows.
- The thickness of the material between the radiator and the sensitive volume is reduced. The ineffective absorption of TR photons by this material is one reason for the low TR-photon detection efficiency of the TRD prototype. We reduced this structure to 3 mm of methane and 5 mm of working gas, based on mechanical feasibility.
- Xenon is used as the working gas. Xe-based mixture gas has a higher detection efficiency for TR-photons compared to Ar-based mixture gas.

Considering the limited resources of the detector in orbit, we have carefully selected and optimized the material and parameters of the detector structure. Methane was chosen as the radiator gap gas due to its low self-absorption of TR-photons and lower gas permeability in the PI window compared to CO_2. The total thickness of the radiator was restricted to 10 cm. Based on our calculations, the number of foil layers is positively correlated with the TR-photon yield in a finite radiator thickness. For practical reasons, we chose a gap thickness of 500 μm and a foil layer of 200. Xenon was selected as the working gas, with a sensitive volume thickness of 7 cm, resulting in a total detector thickness of about 20 cm. figure 5(a) shows the number of detectable TR-photons as a function of foil thickness for seven different foil materials. We selected PI as the foil material because of its low out-gassing rate compared to PP, PE, and Mylar. We determined the optimal foil thickness to be 20 μm. figure 5(b) shows the response curve of the side-on TRD. In the saturated region ($\gamma > 10^4$), the number of detectable TR-photons increased from 0.65 (prototype) to 1.99 (optimized) per event.

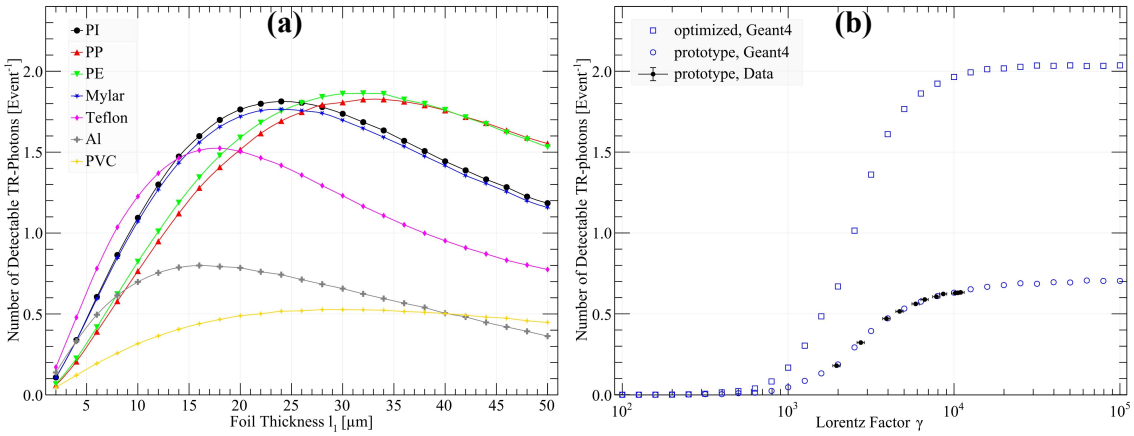

Figure 5: (a) The plot shows the number of detectable TR-photons as a function of foil thickness l_1 for different foil materials. The black circle represents Kapton (PI), the red triangle represents polypropylene (PP), the green reversed triangle represents polyethylene (PE), the blue pentagram represents Mylar, the magenta rhombus represents Teflon, the gray cross represents aluminum (Al), and the orange star represents polyvinyl chloride (PVC). The gap gas in the radiator is methane, the gap thickness is 500 μm, and the foil layer is 200. The detector working gas is Xe : CH_4(90 : 10) at atmospheric pressure, and the depth of the sensitive volume is 70 mm. The Lorentz factor is $\gamma = 5000$. The incident window (100 μm PI) between the sensitive volume and radiator, the field cage (150 μm PI), and the absorption of the non-sensitive region (3 mm methane and 5 mm working gas) are also considered in the calculation. (b) The plot shows the response curves of TRD. The black filled circle represents the beam test data of the prototype, the blue unfilled circle represents the simulation of the prototype, and the blue unfilled square represents the simulation of the optimized detector (the foil is PI with a thickness of 20 μm, other parameters are the same as those calculated in the left figure).

5 Conclusions

A Monte Carlo simulation model based on Geant4 has been constructed to reproduce the THGEM-TRD. In this MC model, Geant4 records the hits information of particles in the sensitive volume of TRD. In digitization, we consider three effects: the transverse diffusion coefficient of electrons in the drift region, which is calculated by Garfield++; the multiplication of electrons in the THGEM hole, which includes the gain coefficient and energy broadening of THGEM; and the offset of the electronics response. We use the model to reproduce the side-on TRD prototype and compare the simulation results with the beam test data. The beam momenta range from 1.0 to 5.6 GeV/c, which covers the linear and saturation regions of the TRD response curve, and the two results are in good agreement. We use the verified MC model to optimize the detector, which can detect three times more TR-photons than the prototype. Additionally, the model can be used to simulate the in-orbit energy calibration of TRD and CALO, as well as the in-orbit background study of TRD.

Acknowledgments

The measurements leading to these results have been performed at the Test Beam Facilities at DESY. The authors would like to thank the HERD collaborators and acknowledge the useful discussions with Qian Liu from the University of Chinese Academy of Sciences, Ming Shao, Zhiyong Zhang and Changqing Feng from the University of Science and Technology of China. This work is supported by the National Key R&D Program of China (2021YFA071840X), the National Natural Science Foun-

dation of China (Grant Nos. 12027803, U1731239, 12133003, 12175241, U1938201, U1732266), the Guangxi Science Foundation (Grant Nos. 2018GXNSFGA281007, 2018JJA110048).

References

[1] S.-N. Zhang, O. Adriani, S. Albergo, G. Ambrosi, Q. An, T. Bao et al., *The high energy cosmic-radiation detection (herd) facility onboard china's space station*, in *Space Telescopes and Instrumentation 2014: Ultraviolet to Gamma Ray*, vol. 9144, p. 91440X, International Society for Optics and Photonics, 2014.

[2] D. Kyratzis, *Herd: The high energy cosmic-radiation detector*, *Il nuovo cimento C* **43** (2020) 1.

[3] F. Gargano et al., *The high energy cosmic-radiation detection (herd) facility on board the chinese space station: hunting for high-energy cosmic rays*, *PoS ICRC2021* **26** (2021) .

[4] D. Kyratzis, H. Collaboration et al., *Overview of the herd space mission*, *Physica Scripta* **97** (2022) 054010.

[5] V. Ginzburg and I. Frank, *Radiation of a uniformly moving electron due to its transition from one medium into another*, *Journal of Physics (USSR)* **9** (1945) 353.

[6] S. Wakely, *Precision x-ray transition radiation detection*, *Astroparticle Physics* **18** (2002) 67.

[7] B. Dolgoshein, *Transition radiation detectors*, *Nuclear Instruments and Methods in Physics Research Section A: Accelerators, Spectrometers, Detectors and Associated Equipment* **326** (1993) 434.

[8] A. Andronic and J.P. Wessels, *Transition radiation detectors*, *Nuclear Instruments and Methods in Physics Research Section A: Accelerators, Spectrometers, Detectors and Associated Equipment* **666** (2012) 130.

[9] X. Liu, B. Huang, H. Feng, H. Liu, W. Xie, X. Huang et al., *Side-on transition radiation detector (trd) based on thgem*, *Radiation Detection Technology and Methods* **4** (2020) 257.

[10] B. Huang, H. Liu, X. Huang, M. Xu, Y. Dong, X. Wei et al., *Side-on transition radiation detector: A detector prototype for tev energy scale calibration of calorimeters in space*, *Nuclear Instruments and Methods in Physics Research Section A: Accelerators, Spectrometers, Detectors and Associated Equipment* **962** (2020) 163723.

[11] J. Gu, H. Liu, X. Huang, B. Huang, M. Xu, Y. Dong et al., *The photon yield efficiency study of transition radiators at e2 line of beijing test beam facility*, *Journal of Instrumentation* **16** (2021) P08041.

[12] Y. Ducros, F. Feinstein, J. Hubbard, P. Mangeot, B. Mansoulié, J. Teiger et al., *Monte carlo simulation of the performance of the d0 transition radiation detector*, *Nuclear Instruments and Methods in Physics Research Section A: Accelerators, Spectrometers, Detectors and Associated Equipment* **277** (1989) 401.

[13] A. Andronic, H. Appelshäuser, R. Bailhache, C. Baumann, P. Braun-Munzinger, D. Bucher et al., *Transition radiation spectra of electrons from 1 to 10 gev/c in regular and irregular radiators*, *Nuclear Instruments and Methods in Physics Research Section A: Accelerators, Spectrometers, Detectors and Associated Equipment* **558** (2006) 516.

[14] T. Räihä, A. Bachlechner, B. Beischer, C.H. Chung, H. Gast, S. Schael et al., *Monte carlo simulations of the transition radiation detector of the ams-02 experiment*, *Nuclear Instruments and Methods in Physics Research Section A: Accelerators, Spectrometers, Detectors and Associated Equipment* **868** (2017) 10.

[15] A. Boldyrev, K. Vorobev, K. Zhukov, S. Konovalov, A. Maevsky, A. Romaniouk et al., *Computer simulation of a transition-radiation detector prototype based on straw proportional chambers*, *Instruments and Experimental Techniques* **61** (2018) 658.

[16] C. Li, C. Feng, D. Zhu, S. Liu and Q. An, *An optical fiber-based flexible readout system for micro-pattern gas detectors*, *Journal of Instrumentation* **13** (2018) P04013.

[17] R. Diener, J. Dreyling-Eschweiler, H. Ehrlichmann, I.-M. Gregor, U. Kötz, U. Krämer et al., *The desy ii test beam facility*, *Nuclear Instruments and Methods in Physics Research Section A: Accelerators, Spectrometers, Detectors and Associated Equipment* **922** (2019) 265.

[18] V. Grichine and S. Sadilov, *Geant4 models for x-ray transition radiation*, *Nuclear Instruments and Methods in Physics Research Section A: Accelerators, Spectrometers, Detectors and Associated Equipment* **522** (2004) 122.

[19] J. Apostolakis, S. Giani, L. Urban, M. Maire, A. Bagulya and V. Grichine, *An implementation of ionisation energy loss in very thin absorbers for the geant4 simulation package*, *Nuclear Instruments and Methods in Physics Research Section A: Accelerators, Spectrometers, Detectors and Associated Equipment* **453** (2000) 597.

[20] *Garfield++, simulation of tracking detectors.*, *Available online: http://garfieldpp.web.cern.ch* (accessed on 1 January 2019) .